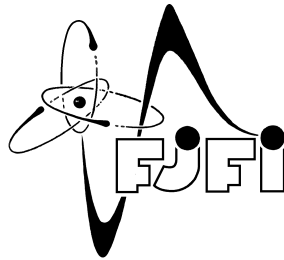


CZECH TECHNICAL UNIVERSITY IN PRAGUE
Faculty of Nuclear Sciences and Physical Engineering



Výzkumný úkol

INSERTABLE B-LAYER PROJECT ON THE ATLAS
EXPERIMENT

AUTHOR:

Bc. Oleksandr Korchak

SUPERVISER:

prom. fyz. Václav Vrba, CSc

August, 2012

Abstract

The ATLAS Pixel Detector is the innermost part of the ATLAS tracking system and is critical for track and vertex reconstruction. In order to preserve the tracking performance in the face of the increasing instantaneous luminosity delivered by the LHC, ATLAS plans to introduce a new pixel layer (IBL) mounted directly on a reduced diameter beam pipe. To cope with the high data rate expected for the IBL a new readout chip (FE-I4) has been designed. Furthermore the IBL will have to sustain an estimated radiation dose, including safety factors, of $5 \times 10^{15} neq/cm^2$. Two sensor technologies are currently being considered for the IBL, the planar n-on-n slim edge and the 3D double sided designs. An extensive evaluation plan which includes device irradiation and beam tests has been carried out to determine the performance of the IBL sensor prototypes. In this thesis the data analysis results from March IBL testbeam at DESY of PPS and 3D (FBK) pixel devices are presented.

Acknowledgments

Author would like to thank the PPS and 3D testbeam group and shifters.
Special thanks for S. Tsiskaridze and I. Rubinskiy.

Contents

1	Introduction	1
2	The ATLAS Experiment	3
2.1	The LHC	3
2.2	The ATLAS Detector	4
2.3	Inner detector	6
2.3.1	The Transition Radiation Tracer (TRT)	7
2.3.2	The SemiConductor Tracer (SCT)	8
2.3.3	The Pixel detector	9
2.4	Insertable B-layer	10
3	PPS and 3D Sensors	12
4	The Test Beam	16
4.1	Introduction	16
4.2	Test beam setup	16
4.3	Runs and configurations	18
5	Track reconstruction overview	21
5.1	Introduction	21
5.2	Format converter	23
5.3	Cluster search	24
5.4	Hit maker	25
5.5	Telescopes and DUTs Alignment	26
5.6	Track fitter	27
6	Data analysis	29
6.1	Offline monitoring software (TBmon)	29
6.2	Analysis Overview	31
7	Analysis of test beam's data	34
8	Conclusions	39

Chapter 1

Introduction

The most important question of contemporary physics is: “What is the matter made of?”

While there were several attempts to answer this question the most acknowledged for today is the Standard Model (SM). According to this model all the matter is build out of fermions, particles called quarks and leptons, with fundamental bosons mediating the interaction between them.

But the theory still contains open issues. The origin of mass is still a mystery. In SM all fermions and bosons are massless. To explain the mass the interaction with a scalar background field is introduced. This interaction requires the existence of a massive scalar Higgs boson with an unknown mass. The Higgs boson is the only particle in the SM that has not yet been discovered, neither found the evidence against its existence.

Alternative approaches such as Supersymmetry has been also proposed awaiting experimental confirmation. To study these and other related problems very high energy particles are needed. For these purposes there were built giant machines like the CERN accelerator complex and the Large Hadron Collider (LHC). One of the experiments run on these techniques is called ATLAS experiment. It requires a very high precision vertex measurement which implies putting detectors as close to the interaction point as possible. The ATLAS collaboration will install an additional inner pixel layer (Insertable B-layer, IBL) mounted directly on top of the beam pipe, at radius of 3.3 cm to increase the performance of the experiment.

The IBL will have to sustain an estimated radiation dose, including safety factors, of $5 \times 10^{15} n_{eq}/cm^2$. Two sensor technologies are currently being considered for the IBL, planar n-on-n slim edge and 3D double sided sensor’s designs.

In this thesis in Chapter 2 presented a short overview of the ATLAS experiment and the Insertabl B-Layer upgrade. Chapter 3 describes different types of silicon pixel sensors. The basic concepts of the test beam setup are

presented in Chapter 4 together with the data taking process. Chapter 5 gives an overview of track reconstruction. Chapter 6 describes the offline data analysis performed. Chapter 7 provides a study and summarizes the results. The conclusions of this thesis are presented in Chapter 8.

Chapter 2

The ATLAS Experiment

2.1 The LHC

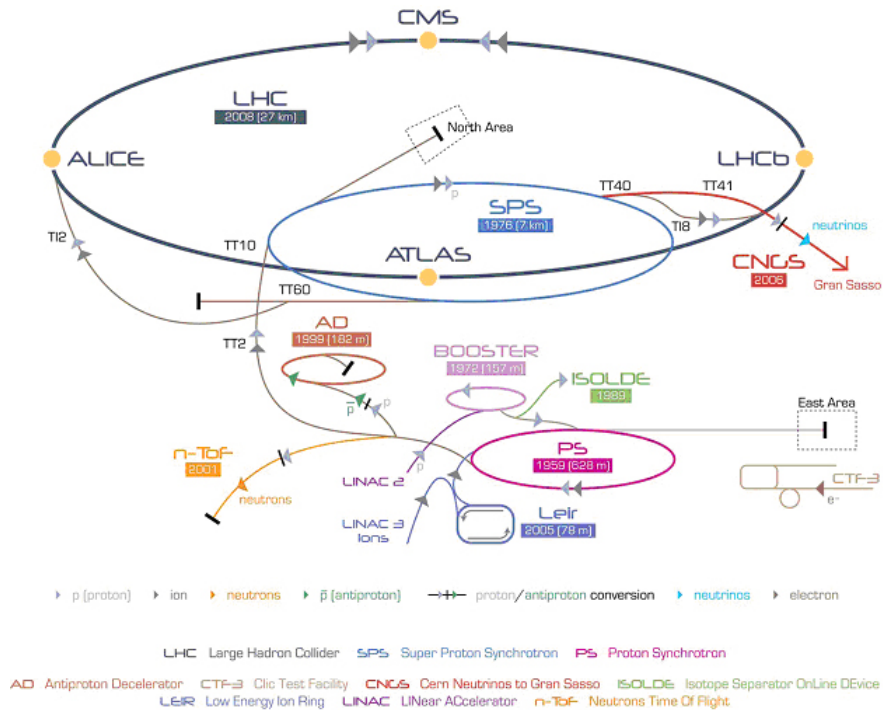


Figure 2.1: LHC (Large Hadron Collider) at CERN

The Large Hadron Collider (LHC), the world's largest and most powerful particle accelerator is the latest addition to CERN's accelerator complex. It mainly consists of a 27 km ring of superconducting magnets with a number

of accelerating structures to boost the energy of the particles along the way (see Figure 2.1). The particles accelerated up to energies of 3.5 TeV are protons. Two beams circulate in opposite directions and are steered into collision at four points along the machine. At these interaction points the protons collide at a total energy of 7 TeV.

There are six experiments at the LHC, all run by international collaborations. Each experiment is distinct, characterized by its unique particle detector. The two largest experiments, ATLAS and CMS, are general-purpose detectors to analyze the myriad of particles produced by the collisions in the accelerator. They are designed to investigate the largest range of physics possible. Having two independently designed detectors is vital for crossconfirmation of any new discoveries made.

The ATLAS detector is installed in a huge underground cavern located at one of the interaction points of the LHC.

2.2 The ATLAS Detector

ATLAS [1] is one of two general-purpose detectors at the LHC. It is investigating a wide range of physics, including the search for the Higgs boson, extra dimensions, and particles that could make up dark matter.

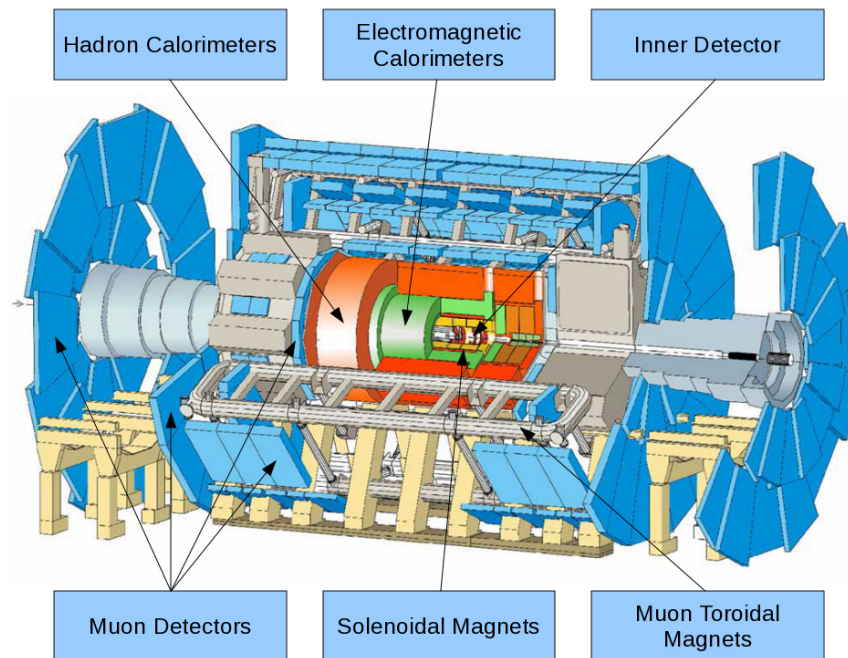


Figure 2.2: The ATLAS particle detector.

When a collision which may be of interest occurs, this usually means that some heavy and therefore short-lived particle or resonance has been created. In general these short lived particles quickly decay into two or more new particles, which in turn continue into the detector. These new particles carry information from the original underlying event which produced them, and the purpose of ATLAS detector is to record as much information as possible about the outgoing particles.

This is accomplished in ATLAS through different detecting subsystems that identify particles and measure their momentum and energy (see Figure 2.2):

- **Inner Detector:** made from highly segmented silicon strips and Pixel detectors responsible for measuring the charged particles trajectories.
- **Hadron Calorimeter:** a device that measures the total energy of hadrons.
- **Electromagnetic calorimeter:** a device that measures the total energy of "electromagnetic showers" produced by electrons, positrons and photons.
- **Muon Detector:** a muon detection system consisting of precision drift tubes, resistive plate chambers, cathode strip chambers and thin gap chambers inside a toroidal magnetic field.

The reason that detectors are divided into many components is that each component tests for a special set of particle properties. On Figure 2.3 one can see the interactions of various particles with the different components of a detector. Each particle type has its own "signature" in the detector. For example:

- Charged particles, like electrons and protons, are detected both in the tracking system and the electromagnetic calorimeter.
- Neutral particles, like neutrons and photons, are not detectable in the tracking system. Photons are detected by the electromagnetic calorimeter, while neutrons are evidenced by the energy they deposit in the hadron calorimeter.
- Muons are detected in all components of the detector.
- Neutrinos are not seen by any of the detectors because they rarely interact with matter and their presence is inferred by missing energy.

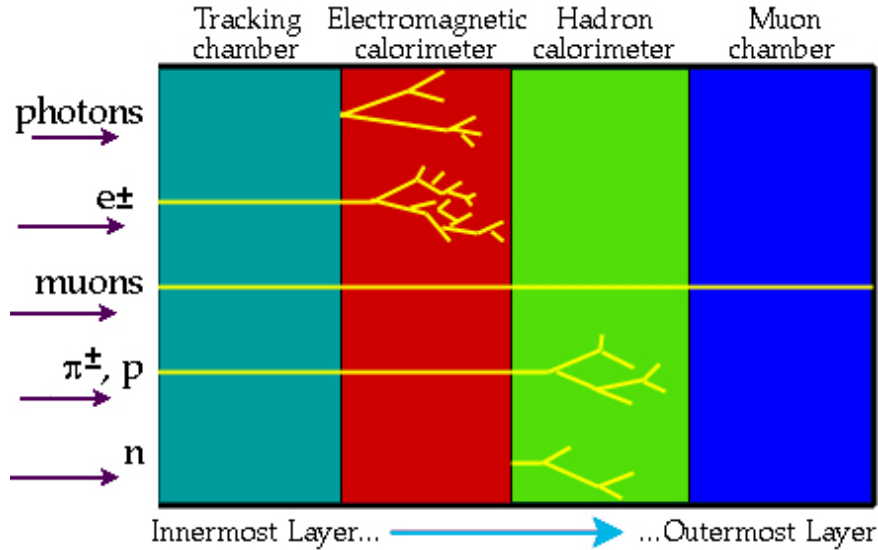


Figure 2.3: The "signature" of various particles in the detector.

2.3 Inner detector

The Inner Detector [2] is crucial to accomplish the ATLAS physics goals. It is designed for precise tracking of charged particles which result of the collision of proton bunches, which occur every 25ns. The detector operates in a nearly homogeneous magnetic field of 2 T provided by a solenoid in order to measure the momentum of the charged particles. It combines tracking straw tubes in the outer transition-radiation tracker (TRT) and microstrip detectors of the semiconductor tracker (SCT) in the middle with the Pixel Detector, as the innermost components. Silicon detectors were chosen for the innermost detector layers because of their radiation hardness and their fine granularity which translate into excellent impact parameter resolution. In order to obtain a larger number of track hit points the silicon detectors are complemented by a detector based on gas-filled elements in the outer radius, where the track density is no longer a problem. Typically for each track the pixel detector contributes three space points and the strips four points. At larger radii about 36 tracking points are provided by the straw tube tracker.

The outer radius of the Inner Detector is 1.15 m, and the total length is 7 m. In the barrel region the high-precision detectors are arranged in concentric cylinders around the beam axis, while the end-cap detectors are mounted on disks perpendicular to the beam axis. The barrel TRT straws are parallel to the beam direction. All the end-cap tracking elements are located in planes perpendicular to the beam direction. A Schematic picture of the inner detector is shown in Figure 2.4

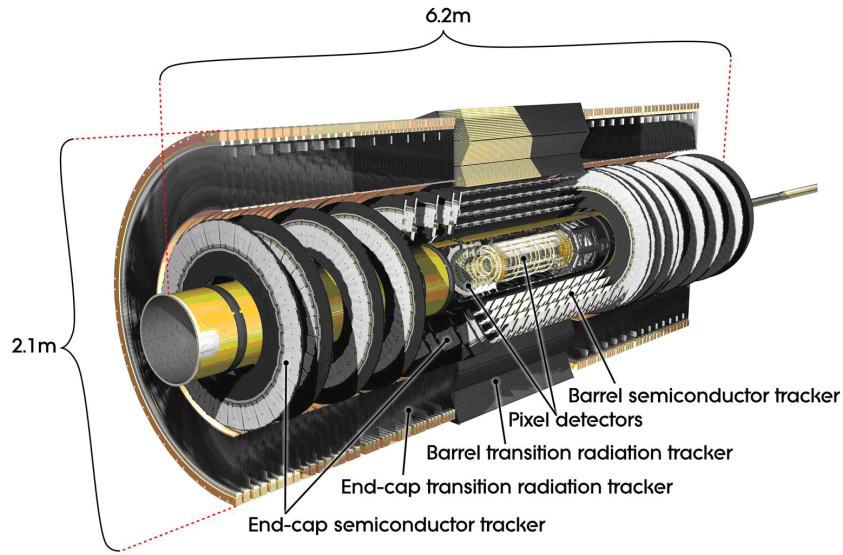


Figure 2.4: ATLAS Inner detector.

2.3.1 The Transition Radiation Tracker (TRT)

The TRT is the outermost part of the Inner Detector. It provides charged-particle tracking based on the use of straw detectors with 420 000 readout channels, as well as electron identification through transition radiation measurements. Electron identification capability is added by employing Xenon gas to detect transition radiation photons created in a radiator between the straws. The TRT consists of a 144 cm long cylindrical barrel layer ranging from 56 to 108 cm in radius and two end-caps ranging from 84 to 271 cm in Z and 64 to 103 cm in radius. Both barrel and end-cap parts contain similar carbon-polyimide straw tubes of 4 mm in diameter which are equipped with a $30\mu\text{m}$ diameter gold-plated W-Re wire. The straws are filled with non-flammable gas mixture of 70% Xe, 27% CO_2 and 3% O_2 , the first component being the main gas in which ionization occurs and the latter had to be added to avoid etching problems with the glass joints that hold the wires.

The straws are operated in proportional mode with the electrodes being on approximately 1530 V bias. The 52544 straws in the barrel form two modules embedded in polypropylene radiator foils in which transition radiation is produced. These modules are then formed into three rings to compose the entire barrel such that the straws are parallel to the Z-axis. The end-caps are composed of 160 planes of 122880 radially arranged straws of 37 cm length.

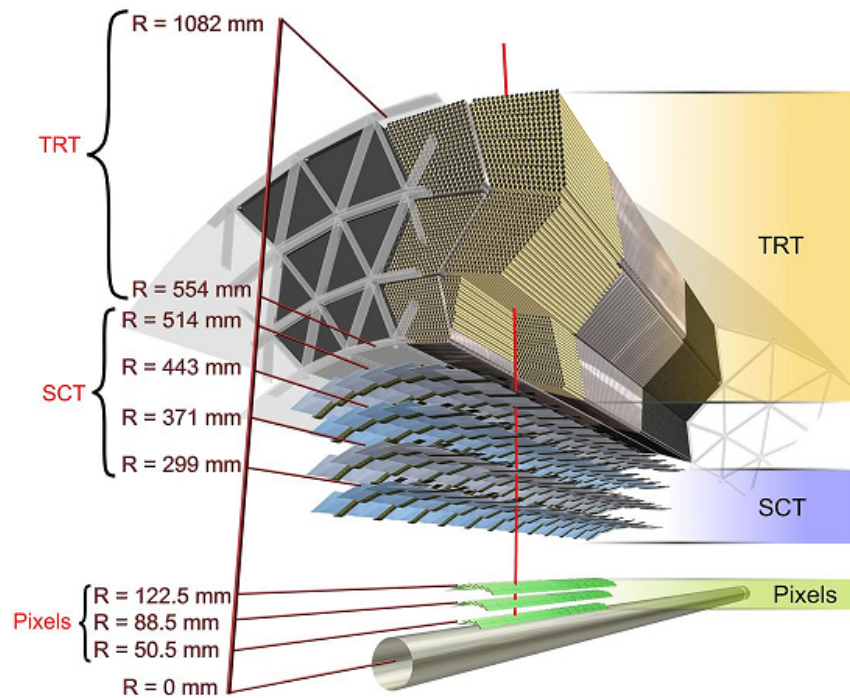


Figure 2.5: Schematic view of the ATLAS inner detector.

The space between each pair of planes is filled with polypropylene radiator.

2.3.2 The SemiConductor Tracer (SCT)

The semiconductor tracer forms the middle subdetector of the inner system. It consists of four nested cylindrical barrels in the center and nine disks in each of the two end-caps (see Figure 2.5). The barrels cover a region from 30 to 52 cm in radius and have an active length of 153 cm, centered around the interaction point. The respective barrel layers are fully covered by 32, 40, 48, and 56 rows of twelve identical modules, overlapping in a tile-structure in order to ensure full coverage, making a total of 2112 modules. The end-caps consist of nine disks each placed between $Z=83.5$ to $Z=278.8$ cm and radii ranging from 25.9 to 56.0 cm. The modules are placed in three rings overlapping azimuthally, two on one side, one on the other, in order to achieve full coverage.

The SCT barrel modules are made of four sensors, glued in pairs on either side of a thermally highly conductive baseboard. The sensors are approximately $6 \times 6 \text{ cm}^2$ p-in-n silicon wafers of approximately $300 \mu\text{m}$ thickness. Each sensor has 768 strips with $80 \mu\text{m}$ pitch.

The end-cap modules are made of two or four wedge-shaped sensors of varying size depending on their position on the end-cap rings. The strip pitch varies from $57 \mu\text{m}$ on the inner edge of the innermost sensors to $94 \mu\text{m}$ on the outer edge of the outermost sensors. The sensor pairs are mounted on a thermally highly conductive carbon base board that provides cooling. The SCT sensors are operated at -7°C to prevent reverse annealing radiation damage.

2.3.3 The Pixel detector

The ATLAS Pixel Detector provides a very high granularity, high precision set of measurements close to the interaction point (see Figure 2.6). The need to precisely measure the momentum of charged particles require fine granularity of the detector segments which silicon detectors can provide. The Pixel Detector is subdivided into three barrel layers in its center, at radii of 50.5, 88.5, and 122.5 mm, and three disks on either side for the forward direction, at a distance of 49.5, 58, and 65 cm from the center of the detector; a drawing of the layout is also shown in Figure 2.5. With a total length of approximately 1.4 m it typically detects three hits per traversing particles with $|\eta| < 2.5$, with the transition between barrel and disk structures being at $|\eta| \approx 1.9$.

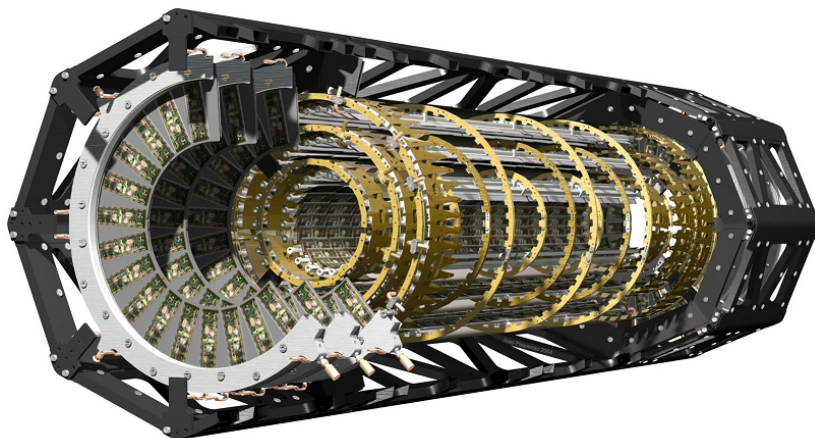


Figure 2.6: ATLAS Pixel Detector.

The Pixel Detector faces the highest amount of particle flux due to its

closeness to the beam pipe, corresponding to the largest radiation damage and hit occupancies in ATLAS. This results in stringent requirements to read-out speed and radiation hardness.

2.4 Insertable B-layer

The current ATLAS detector was designed to be operated at a luminosity of $1 \times 10^{34} \text{cm}^{-2} \text{s}^{-1}$ and to be able to take data up to an integrated luminosity of $500 - 700 \text{fb}^{-1}$. After the successful commissioning of both accelerator and detector, it is planned to further increase the LHC's luminosity from $1 \times 10^{34} \text{cm}^{-2}$ up to $5 \times 10^{34} \text{cm}^{-2}$ in the coming years. Increasing luminosity would enable the LHC detectors to take some 1000fb^{-1} of data in a rather short period of time which significantly extends the LHC's physics reach.

To be able to cope with the luminosity increase, the Inner Detector needs to be upgraded. The ATLAS Collaboration will install an additional innermost layer, the so-called insertable B-layer (IBL) [3], in the current pixel detector during the LHC shutdown currently planned for 2013-2014. This fourth layer will compensate the expected performance deterioration of the current innermost layer and improve the impact parameter resolution.

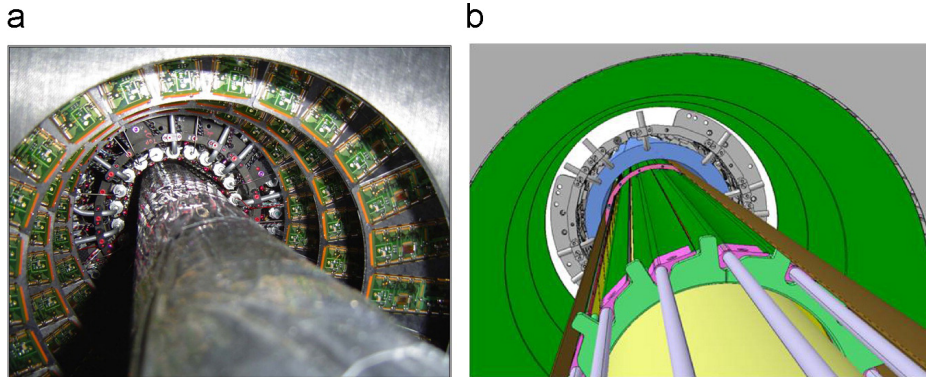


Figure 2.7: (a) Photo of the Pixel Detector with the inserted beam pipe during the integration of the present detector and (b) rendering of the insertion of the IBL with the smaller beam pipe

There are several tough constraints that have to be satisfied by the IBL design. In the first place, the space available is very tight, the outside envelope of the IBL has to have a radius not larger than 43.5 mm. This space needs to fit the beam pipe (with an outer envelope radius of 30 mm), sensors, electronics, services, and support structures. In the second place, the material budget should be kept as low as possible, in order to minimize inter-

ference with detector layers further from the interaction point. Finally, the sensors should be positioned very close to the interaction point, increasing the radiation load and particle density. Until complete replacement of the entire inner detector for HL-LHC in 2020 or later, the IBL will have to sustain an estimated radiation dose, including safety factors, of $5 \cdot 10^{15} \text{ neq/cm}^2$, or 250 Mrad. This means that radiation hard detectors which are able to cope with high particle multiplicities are needed. There are two candidates for the IBL sensor components: planar pixel sensors (PPS) and 3D sensors. These sensors are described in more details in the next Chapter 3.

Chapter 3

PPS and 3D Sensors

Two sensor technologies are being considered for the IBL, planar and 3D sensors (75% Planar and 25% 3D sensor layout) (see Fig. 3.1). Differences between 3D and planar segmented sensors in geometry and charge collection are shown on Figure 3.2.

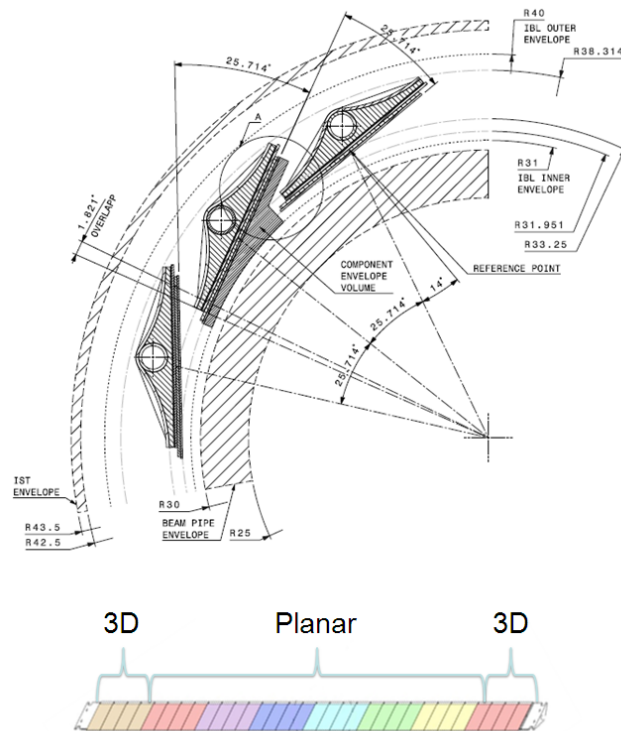


Figure 3.1: Cross section detail of the IBL (top). The 14 staves are mounted directly on the beam pipe. The figure below shows a possible stave layout which combines planar and 3D sensor technologies. [17]

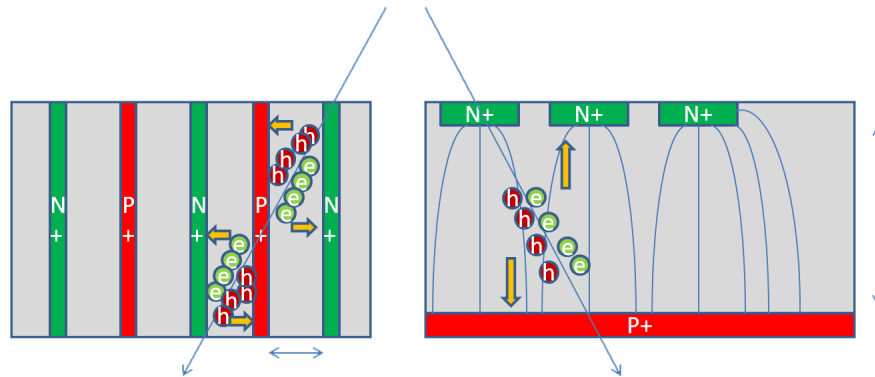


Figure 3.2: Differences between 3D and planar segmented sensors in geometry and charge collection [15]

Planar modules consist of 2-chip assemblies while 3D modules consist of a single chip. Both module designs offer similar nominal acceptance. However, the requirements of the two technologies in terms of temperature and bias voltage differ, being less restrictive for 3D sensors. Both technologies have to demonstrate that they satisfy the IBL requirements in terms of performance after irradiation to $5 \times 10^{15} n_{eq}/cm^2$. Planar and 3D sensors with the IBL design have been fabricated, and have been interconnected (bump-bonded) with the FE-I4 read out chip. These planar and 3D bare assemblies were wire-bonded to an electronic card to carry out the characterization and test-beam studies need to evaluate the technologies. The wire-bonded devices are also referred to as single chip assemblies.

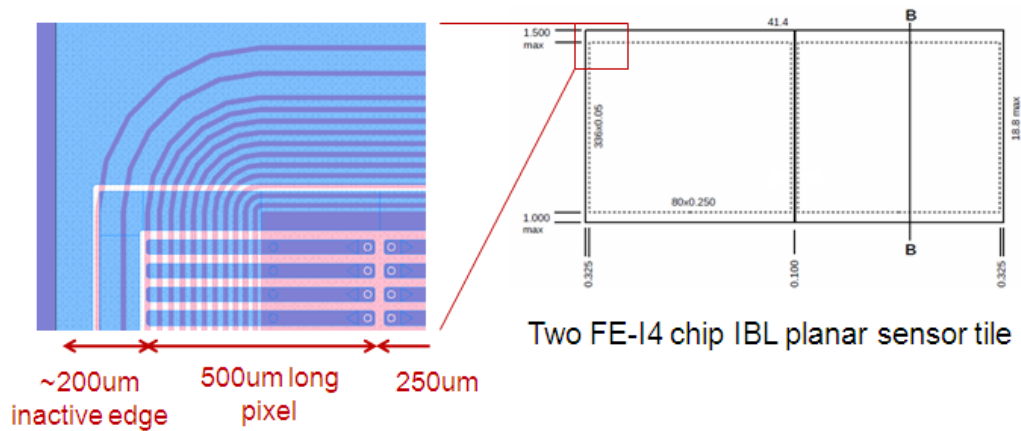


Figure 3.3: Planar sensor IBL design [4]. Planar modules consist of two front end readout chips. The detail on the left shows the edge pixels which extend over the ohmic side guard rings to provide an inactive edge of about $200 \mu m$.

Planar Pixel Sensors. The IBL planar sensors rely on the proven technology of the current ATLAS Pixel Detector [17], n-on-n pixels on a diffusion oxygenated float-zone silicon bulk. The chosen thickness for the substrate is $200\mu\text{m}$, a sizable reduction from the $256\mu\text{m}$ featured in the current Pixel Detector. Isolation between the n+ implants is obtained through the moderated pspray technique. A bias grid is integrated into the design to determine the sensor electrical quality before bump-bonding. In order to reduce the inactive edges, the planar IBL design shifts the guard rings on the ohmic side beneath the outer pixels. To keep the sensor length constant, the edge pixels are extended to $500\mu\text{m}$ (see Fig 3.3).

A distortion on the electric field on the sensor edge will be introduced by this layout, but the charge collection after irradiation occurs primarily in the region directly beneath the n^+ implant. The inactive edge of planar devices achieved with this design is around $200\mu\text{m}$

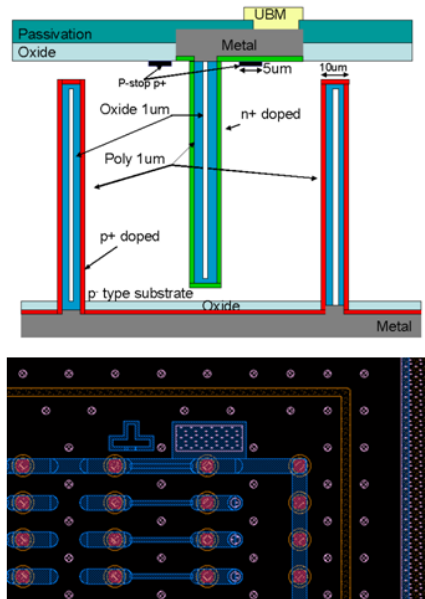


Figure 3.4: Design of the CNM 3D sensors (top) [18]. The electrodes do not penetrate the full thickness of the sensor. Below a detail of the production mask is shown. The two electrode configuration is visible as well as the 3D guard fence.

3D Sensors. The 3D pixel sensor design exploits recent silicon technology advances to produce column-like electrodes that penetrate the substrate, instead of being implanted on the wafer surface [17]. The depletion region thus grows parallel to the wafer surface. The $\approx 10\mu\text{m}$ diameter columns are alternatively n and p-type doped defining the pixel configuration. The

3D design is intrinsically radiation hard since it decouples the electrode distance from the bulk thickness, making possible the reduction of the charge collection path without reducing the amount of sensor material the charge particles traverse. IBL 3D sensors have been manufactured in two production facilities, CNM (Spain) and FBK (Italy), with the same specifications.

The sensors are produced on a $230\mu\text{m}$ thick wafer with a double sided process, i.e. the n- and p-type columns are etched from the opposite sides of the substrate. The pixel configuration consists of two n-type readout electrodes connected at the wafer surface along the $250\mu\text{m}$ long pixel direction, surrounded by six p-type electrodes which are shared with the neighboring pixels, see Fig. 3.3

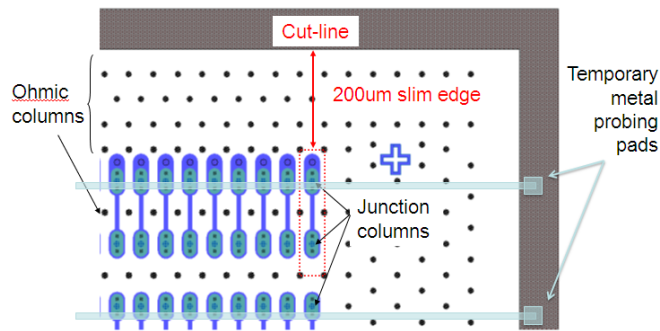


Figure 3.5: Detail of the FBK 3D design [17]. The temporary metal strips are used to evaluate the electrical characteristics of the device before bump-bonding.

The CNM 3D sensor design features $210\mu\text{m}$ long columns which are isolated on the n+ side with p-stop implants. The edge isolation is accomplished with a combination of a n+ 3D guard ring, which is grounded, and fences which are at the bias voltage potential from the ohmic side (see Fig. 3.3)

The inactive edge region is about $200\mu\text{m}$ long. The sensor quality before wafer dicing is evaluated on the 3D guard ring. The FBK 3D sensor design presents pass-through columns isolated on the junction side with the p-spray technique. A $200\mu\text{m}$ long ohmic fence isolates the pixel area from the edges in the z direction. The sensor quality is evaluated before dicing using a temporary metal line that connects 336 pixels into a strip, see Fig. 3.4. A total of 80 strips that are connected to a probing pad located outside the active region of the sensor, allow to evaluate the electrical characteristics of the device.

Chapter 4

The Test Beam

4.1 Introduction

Critical performance parameters, such as hit efficiency and position resolution, can only be determined at beam tests. Planar and 3D IBL devices were studied on the DESY supersynchrotron machine, which provides positrons with energy of 4 GeV/s. The trajectories of the beam particles are recorded using a reference system (Telescope). Since the positrons have a high kinetic energy they may be considered as minimum ionizing particles (MIPs), and thus, the multiple scattering effects can be neglected. This allows to perform high precision tracking measurements. Devices Under Test (DUT) are placed in the beam trajectory. Track positions in telescope planes and information from the DUT itself and the arrival time of the particles allow to characterize the devices, estimating hit reconstruction efficiency and resolution.

To carry out such measurements is using test beam setup like that as shown in Figure 4.1. While the details of a testbeam setup vary for different applications, the basic concept is usually the same. The test beam setup which was used for this thesis is described below in detail.

4.2 Test beam setup

The EUDET Pixel Telescope [7] was used for track measurements. The detector planes of the telescope consisted of Mimosas26 pixel sensors. Among of 576×1152 pixels cover an active area of $10.6 \times 21.2 \text{ mm}^2$ with a $18.4 \times 18.4 \text{ }\mu\text{m}^2$ pitch. Six telescope planes were equally distributed into two upstream

and downstream arms. During measurements the distance between the arms was 40.1cm . The telescope resolution is approximately $3\ \mu\text{m}$. To increase the precision of detecting the hit positions, the devices under test (DUTs) were placed between the telescope arms. Some of them were kept in a cooling box at an operation temperature of about -15°C . The data were taken with the incident angles at 0° and 15° .

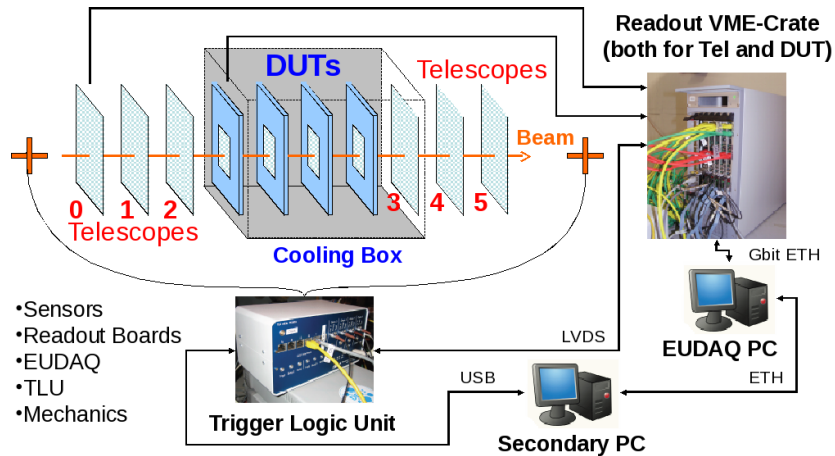


Figure 4.1: The test beam setup

The data from DUTs are read out by USBpix System [8] and sent to the main DAQ PC. The telescope sensors are read out by custom readout electronics that have been adapted to read out the fully digital MIMOSA-26 sensors. The maximum rate of the full setup with two VME crates reading out 3 Mimosa26 sensors each using the 80MHz clock is about 800Hz . The passage of particles was triggered by using upstream and downstream mounts of two $1 \times 2\ \text{cm}^2$ scintillators at right angles. Triggering is controlled by a custom Trigger Logic Unit (TLU) that receives signals from scintillators in front of and behind the telescope, and generates triggers that it distributes to the telescope and any DUT. For each generated trigger a trigger counter is incremented, and a timestamp is stored in an internal buffer that may be read out over USB by a PC. The DUTs have the option to read out the trigger number via the DUT interface in order to ensure proper synchronization of triggers.

For Data Acquisition (DAQ) a custom framework, called EUDAQ, is used. It provides graphic interface to the users allowing them to monitor the quality of data taking. The data recorded from the telescope and devices under test during one trigger are called an event. A sequence of events without changes in the setup or re-initialization of the data acquisition system is referred to as a run.

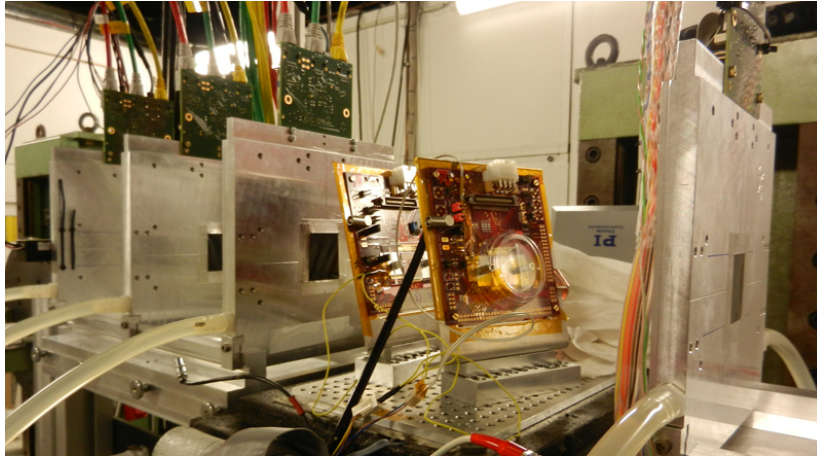


Figure 4.2: The DUTs planes

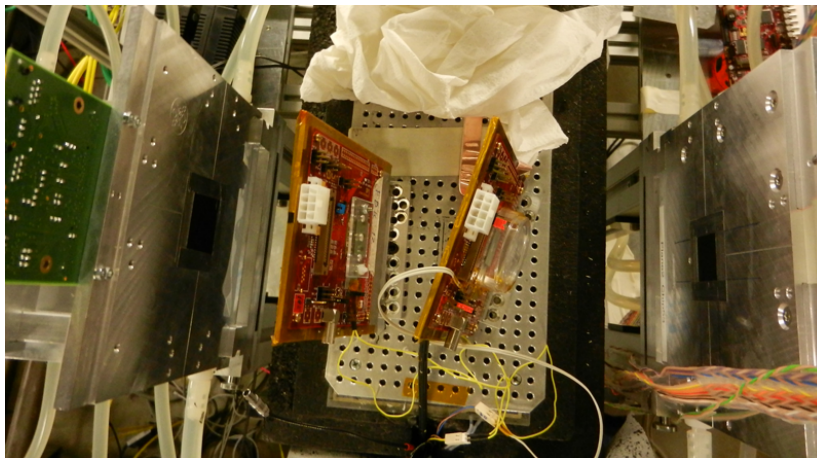


Figure 4.3: The DUTs planes, a top view

4.3 Runs and configurations

In this thesis the results of the measurements performed during the March 2012 beam testing period at DESY are presented.

The goal of the beam tests is to evaluate the performance of different devices (sensors and readout electronics) under IBL conditions (angle, magnetic field, temperature, etc.). To be able to compare the performance of different devices, they were installed side by side and tested simultaneously. Due to the large number of samples to be tested, the beam test period was divided into several batches with different configurations.

Tables 4.1,4.2 describe the batches from March test beam wich was re-constructed and then analysis in this thesis.

Sensor Type	FBK11	FBK13
DUT ID	20	21
Board ID	200	206
Fluency, [n_{eq}/cm^2]	p-irrad: $6.8 \cdot 10^{15}$	un-irrad
ϕ	0	0
η	15	15
Threshold	$1500 e^-$	$1500 e^-$
HV	-120 V	-30 V
HV	-140 V	-15 V
HV	-150 V	-20 V
HV	-160 V	-25 V
Threshold	$1800 e^-$	$1800 e^-$
HV	-140 V	-15 V
Threshold	$2000 e^-$	$2000 e^-$
HV	-140 V	-15 V

Table 4.1: Configuration, Batch2

Sensor Type	PPS75	PPS31
DUT ID	20	21
Board ID	200	206
Fluency, [n_{eq}/cm^2]	p-irrad: $6.8 \cdot 10^{15}$	un-irrad
ϕ	0	0
η	15	15
Threshold	$1500 e^-$	$1500 e^-$
HV	-1000 V	-100 V
HV	-800 V	-100 V
HV	-600 V	-100 V
Threshold	$1800 e^-$	$1500 e^-$
HV	-600 V	-100 V
Threshold	$2000 e^-$	$2000 e^-$
HV	-600 V	-100 V

Table 4.2: Configuration, Batch4

In these tables the following legend is used:

- **DUT ID:** the ID of the device under test used for reconstruction and analysis.
- **Fluency:** the irradiation type and fluency of the sensor: un-irradiated, p-irradiated or n-irradiated.
- **Threshold:** the minimum charge (in number of electrons) that has to be collected by the device to fire the front-end discriminator.
- **HV:** the Bias Voltage of the sensor used during data taking.
- ϕ : the rotation angle of the sensor in ZY plane (Along the long pixel direction).
- η : the rotation angle of the sensor in ZX plane (Along the short pixel direction).

Chapter 5

Track reconstruction overview

5.1 Introduction

When testing pixel detectors the first task is to determine as precisely as possible the so called *hit-point* - the point of intersection of the particle trajectory with the DUT (Device Under Test) plane. The hit points are then used to evaluate essential parameters of the DUT, such as tracking efficiency, resolution, etc. To calculate the position on the DUT plane one has first to reconstruct the trajectory of the particle using the hits from the reference detectors of the telescope system.

As it was already mentioned, both telescope and DUTs sensors represent a set of read out pixel cells collecting the charge deposited by passing particles. When the charge value collected by a pixel is higher than the designated charge threshold, this is registered by the detector software as a hit and the appropriate information is recorded, including pixel coordinates and signal arrival time. In the case of the DUTs, the amount of time the signal exceeded the threshold value (Time over Threshold or ToT) is also recorded. Threshold and TOT are tuned individually in each pixel of the sensor. The pixel that gives signal above threshold is said to have "fired".

Due to charge sharing not only one particular pixel but often also some of the neighboring pixels may overpass the charge threshold and fire. All fired pixels having shared the charge deposited by a passing particle form a connected entity of cells called a cluster.

The first task in track reconstruction is to assemble fired pixels into clusters. There are several issues that complicate the task at this stage: some red pixels may be produced by electronic noise ("noise" pixels), others may be damaged and fire constantly ("hot" or "noisy" pixel) or never ("dead" pixel). The "noise" and "hot" pixels produce additional clusters or affect the

shape of the existing ones. On the other hand, simply discarding ("killing") hot pixels may result in cluster shape distortion and even in splitting a cluster into disjoint parts. Distortions may be caused also by "dead" pixels.

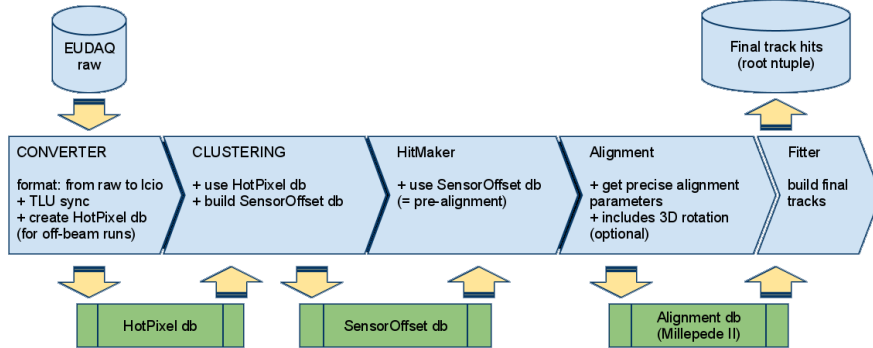


Figure 5.1: Data reconstruction steps [16].

After the clusters are reconstructed in an appropriate way in all sensor planes (telescope and DUT), the next task is to estimate actual hit positions. This challenge is called "cluster centering" and several algorithms have been proposed so far to resolve it, none of them being indisputably preferable. The simplest solution is to calculate the geometrical center of the cluster, in other words, the center of masses of fired pixels assuming they have equal masses. This method is used for the clusters from the telescope planes. In DUTs, where the ToT values for fired pixels are stored in the database, one may try a ToT weighted center of masses where each pixel is assumed to have a mass proportional to the pixel ToT. A more complicated approach is demonstrated in the η - *correction* method which tries to statistically correct the distortion introduced by the uncertainty in the exact hit position.

While several clusters in different sensor planes are required for track fitting, the relative position and orientation of the telescope and DUT planes themselves are not known with enough precision from the survey of the test-beam setup. The possible solution is to perform preliminary track fitting using clusters centers and then to use the fitted tracks parameters from a good number of the run events to align the telescope and DUT planes simultaneously. The adjusted alignment information may then be used to correct the hit positions for tracks reconstruction. This process is repeated until no further adjustment is needed. This approach allows to iteratively adjust both the telescope planes alignment and the tracks positioning. It is worth to note that for track reconstruction only the hits from telescope plane are used. The sequence of successive steps during track reconstruction is often called reconstruction chain. The reconstruction chain used in this thesis is based on a so called Marlin framework provided in the ILCSoft package

A typical Marlin analysis is realized in terms of modules which are called track reconstruction processors (or simply Processors). Each processor determines an event-wise processing unit with its initialization, core, and finalization methods. The core is executed once per every event, while the initialization and finalization methods - once per execution. It also provides plots made in ROOT framework [9]. The reported test-beams track reconstruction processors are contained in the EUTelescope library [10]. They are shown in Figure 5.1. On each step of the reconstruction chain the software provides plots for checking the correctness of the reconstruction as a whole. Below each processor is explained in detail.

5.2 Format converter

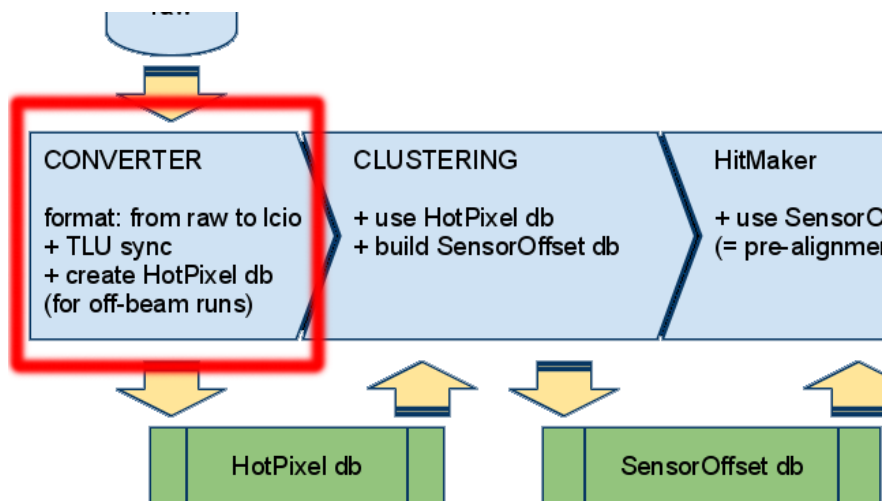


Figure 5.2: Data reconstruction steps. Converter [16].

The first processor in the reconstruction chain called **Format Converter** converts initial raw data into Linear Collider Input/Output (LCIO) format [14]. LCIO is a persistence framework and event data model used by groups involved in linear collider detector studies. At this conversion step no information is dropped nor added to the data. After conversion the data are grouped by events. The information about the DUTs represents a set of data separated by a sensorID and consisting of a sequence of hits represented by five entries per hit. These entries contain the information about the Column, Row, ToT, LV1 Trigger and Readout Identification number of the hit. These values are different for FE-I3 and FE-I4 devices. Column means the column number of the hit which varies from 0 to 79 and Row

means the row number of the hit varying from 0 to 335; ToT is the Time over Threshold value obtained for the hit and may take values from 0 to 15 for FE-I4 devices; LV1 means the Level 1 trigger value indicating when the signal was detected and the Readout identification number contains the number of the readout board from which this information was originated. Similar information is obtained for telescope planes, with the exception that there are no ToT ; and LV1 values.

When the raw data is converted to LCIO format, the Format Converter processor generates a Hot Pixel database file containing the information about noisy pixels of the telescope and DUT planes. This database also has the same LCIO format and contains the information about the noisy (or hot) pixels of the telescope planes. The procedure which removes the hits with noisy pixels is called **Hot Pixel Killer** (HPK). This procedure is crucial for track reconstruction because, as indicated earlier, the noisy hits may create additional track candidates and affect not only the alignment process but also the final track reconstruction results. They also create a combinatorial background that increases the processing time. It was decided to perform only the hot pixel killing for the telescope planes to avoid losing useful information about hits from the devices under test.

Since the beam is not uniform in the XY plane, obtaining hot pixel maps from the real beam data is affected by the beam and it was decided to take a calibration run for the HPK without the beam. The resulting HPK database file for telescopes is then used for all real runs.

5.3 Cluster search

As mentioned before, when a particle passes through a sensor it may deposit energy in several pixels at the same time ("fire" pixels). This may happen both for telescope and DUT planes and the next step is to group neighboring pixels that fired at the same time into objects called clusters. The procedure of allocating clusters is called Cluster Search, or Clustering.

In the default configuration the nearest-neighbor search algorithm is used for clustering. It goes through all fired pixels within the event and consolidates neighboring fired pixels into clusters. Each pixel may have up to 8 neighboring pixels. All fired neighbors for a given fired pixel are added to the current cluster and the clustering procedure recursively applied to all fired pixels of the cluster until there are no fired neighbors. As a result, this recursive procedure ends having grouped the neighboring fired pixels into disjoint clusters. After the clusters are marked out, the hit position is evaluated as a cluster center by a processor called Hit Maker.

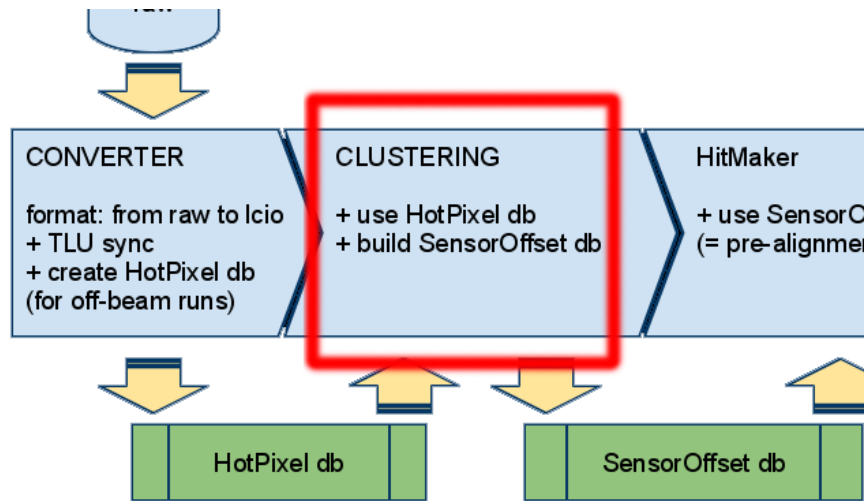


Figure 5.3: Data reconstruction steps. Cluster search [16].

It is worth noting that clusters which are neighboring any masked pixel are not considered in the further reconstruction chain.

5.4 Hit maker

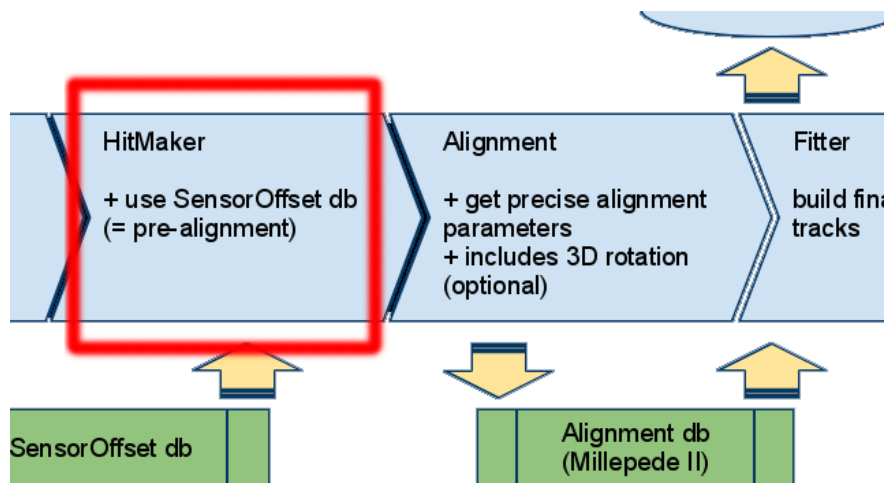


Figure 5.4: Data reconstruction steps. HitMaker [16].

Since the pixel pitch of the telescope differs from that of the DUTs, the cluster position have to be recalculated in the telescope global frame. This is a right-hand Cartesian "XYZ" system, where the telescope reference sensors are located in the XY plane and the sensors are centered at x=0 and

$y=0$. The Z axis of the system follows the direction of the beam and in the default setup of the telescope it is perpendicular to the sensor planes. To process the cluster, a 3-dimensional point called cluster center is used. Using the Geometry file which provides the basic information about detector planes and testbeam setup, the cluster center positions in a global reference frame are calculated. This is performed by the HitMaker processor, which additionally provides the correction constants for an initial alignment of the sensors. These constants are saved in the "pre-alignment" database file.

There are several algorithms to calculate the hit-point position:

- **Cluster Weighted Center**

The simplest method for calculating a cluster center is to take an average of the coordinates of the cluster pixels separately for X and Y. Since the fired pixels coordinates are only known for the telescopes this method is used to evaluate the hit position for clusters from telescope planes. Note, that if the cluster consists of one pixel only, the uncertainty of the telescope hit-point will be:

$$\sigma_{hit-point} = \frac{d_{pitch}}{\sqrt{12}} \approx 5.311\mu m \quad (5.1)$$

where $d_{pitch} = 18.4\mu m$ is the width of the square pixels of the telescope planes.

- **Cluster Charge Weighted Center**

If the charge collection from the Time-over-Threshold information is available, one can use it to adjust the hit-point position for the cluster of the DUTs. This may be done by attaching the corresponding weights to the centers of the pixels and taking the center of mass of the obtained points as the hit-point position. HitMaker uses this method for the DUTs.

Note that if the cluster consists of one pixel only, this method gives the same result as that Cluster Weighted Center. But if there are several hits inside the cluster, the resolution of the hit is expected to be better.

5.5 Telescopes and DUTs Alignment

The alignment of the telescope and DUT planes is carried out in two steps. At the first step ("pre-alignment") the telescope and DUT planes

are only aligned in X and Y directions, within $100\ \mu\text{m}$. The "pre-alignment" constants for all sensors are calculated with respect to the first upstream sensor and provided by the HitMaker. The procedure operates with hit coordinates in the global telescope frame so that it could be applied to sensors with different pixel geometry and different sensor tilts. The pre-alignment constants can be used as correction factors for the sensor positions or as input parameters for the second "fine" part of the alignment process.

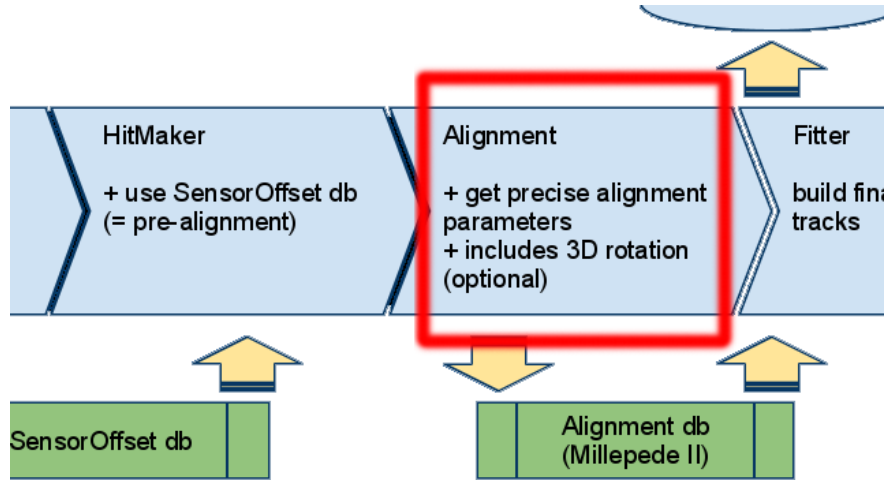


Figure 5.5: Data reconstruction steps. Alignment [16].

Using appropriate criteria, the hit positions from different sensor planes are grouped in track candidates and passed to a Millepede II [15] program, which returns the alignment constants for each sensor based on the Linear Least Square algorithm. These constants represent the sensor shift corrections in X, Y, Z coordinates as well as the 3 Euler rigid body rotation angles and are saved in an "alignment" database file and with the "pre-alignment" constants are used as final corrections for calculating hit positions.

Note that proper handling of hot pixels is crucial for alignment of noisy sensors, in irradiated devices or during lower threshold operation.

5.6 Track fitter

Finally, with the aligned sensors it is possible to reconstruct the particle trajectory. Track reconstruction is performed by Track Fitter processor which relies on Deterministic Annealing Filter (DAF) for track reconstruction. DAF can be viewed as a standard Kalman Filter where all hit-points from telescope planes (not the DUTs) participate in the track reconstruction. The Track Fitter processor works as follows:

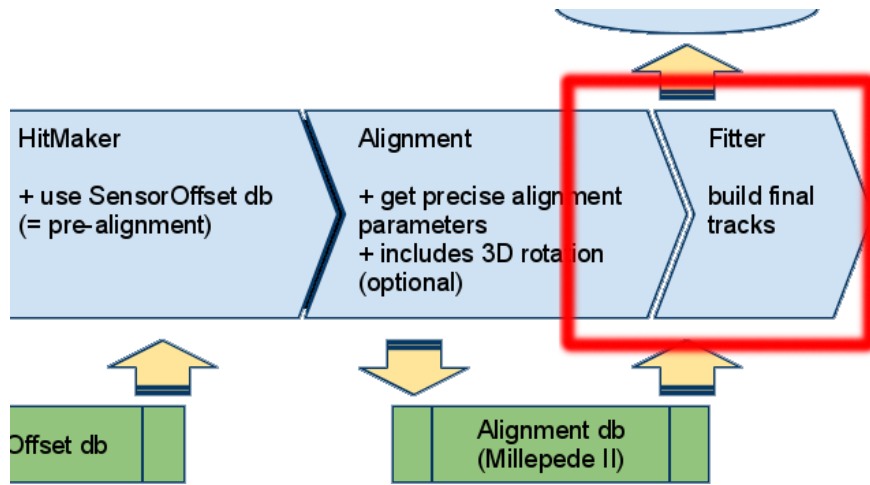


Figure 5.6: Data reconstruction steps. Fitting [16].

1. Propagates all hits into the first "upstream" plane by using the user supplied angles.
2. Run a cluster finder on hits based on the user supplied radius.
3. Run the DAF on the found hit clusters.
4. Checks that the fitted tracks contain a sufficient amount of telescope hits.
5. Checks that the χ^2/ndof of the fitted track is ok.
6. Checks that the track matches a sufficient amount of DUT hits.

TBtrack.root file

The reconstructed tracks and corresponding information about initial raw hits from the DUT planes are stored in a ROOT called TBtrack. These files are further processed to obtain the final device performance results. Note that raw information from DUT planes is kept to perform the offline analysis.

Chapter 6

Data analysis

6.1 Offline monitoring software (TBmon)

TBmon [11] is an offline analysis framework for the ATLAS 3D pixel test beams, based on C++, developed inside the 3D community. The main purpose of the TBmon is to study the output root files from the track reconstruction and to extract physics results, such as charge collection, tracking efficiency, device resolution, charge sharing between pixel cells, etc. It first perform a new DUT clustering reconstruction and then execute different data analysis routines. For a given set of runs, TBmon allows to extract data from reconstruction files (TBtrack.root file), make specific cuts and calibrations, run different analysis and produce a set of desired plots for all specified devices under test. It is flexible and at the same time modular enough, so that one can run the same analysis on data from different beam telescopes, improves exiting analysis code or develops a new original one and adds it to the framework. TBmon has been chosen by the both 3D and PPS communities to be the official framework to use and to perform in a standard and comparable way the data analysis.

Since there is no DUT cluster information in the TBtrack file, TBmon needs to re run the clustering algorithm. It also performs more precise cleaning of these data. Tbmmon assumes that the data are structured in configurations, which are generally corresponding to one batch or particular test environment. One single configuration is built up of one or several runs, which are TBtrack files containing detector digits and tracking information. In addition to these files, a configuration also contains event builders that handle data I/O for these files and set track flags. The output of an event builder is an event object, which contains all the relevant information for the current event and the device under test, such as vectors of all hits as well

as clusters belonging to the current DUT and the fitted track parameters extrapolated to it.

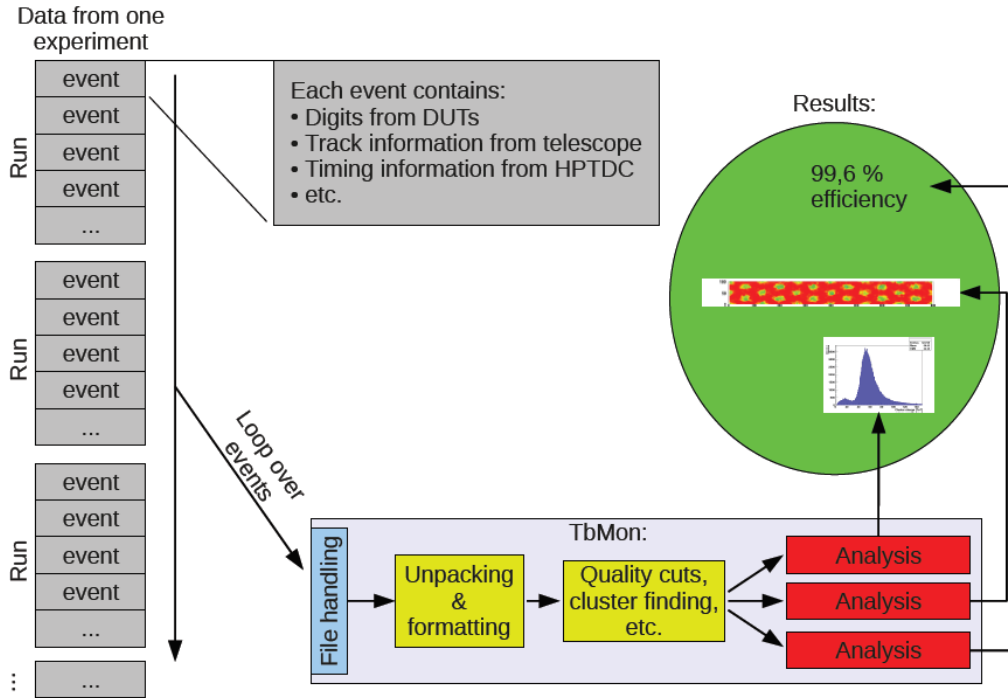


Figure 6.1: TBmon overview: Input, schematical internal structure and Output [12].

The events are built by classes inheriting from the `EventBuilder` class. The following are the most commonly used eventbuilders:

- **EuBuildTrack** which extracts data from root n-tuples and generates appropriate event objects.
- **VL1Cuts** which cuts out the hits when their LVL1 trigger value is out of the manually prescribed window.
- **ClusterFinder** which combines the hits from an event into clusters
- **ClusterMasker** which removes the clusters that are nearby the masked pixels. It also sets the event flag indicating whether some track matches to these clusters
- **CheckRegion** which sets the event flag indicating whether the matching track passes either out of the central region of the sensor or through a masked pixel

These events are then passed on to one or more analysis routines, which make plots and calculations based on the data accumulated for each device under test. The scemtical structure of TBmon is shown in Figure 6.1.

6.2 Analysis Overview

First of all let's define a few usefull terms:

- **Sensor Map** - a map of a sensor as composed of pixels, each pixel being attributed a value of the parameter of interest and being colored according to that value. This kind of plots represent important characteristics of the experiment, such as beam profile, central and edge efficiency, etc.
- **Pixel Map** - it shows cumulative distribution of some parameter mapped over the pixel area. It is helpful when exploring the behavior of the given parameter in the space between neighboring pixels.

The main analyses preformed for the devices are listed below. They are arranged from the simplest to the more complicated ones.

Beam profile sensor map

The Beam profile plots shows the beam position with respect to the DUT by showing the track position on the devices studied. Typically only part of the sensor is covered by the telescope area.

LVL1 trigger distribution

The LVL1 trigger distribution shows the number of readout events as a function of the time after the scintillator triggers initialize the telescope readout. This distribution gives an idea about time synchronization between the telescope and DUT planes. Devices are synchronized to start detecting the signal at around 5 LVL1 values, i.e. after $5 \times 25ns = 125ns$ since the trigger from the scintillators arrives. This distribution also gives an idea about noisy hits: LVL1 values of noisy hits are evenly distributed so that they create a smooth plateau on the LVL1 trigger distribution plot.

Cluster ToT spectrum distribution

The cluster ToT spectrum is the distribution of the deposited charge (in ToT) of the detected particles. It shows the number of readout events as a function of the ToT of the clusters. The ToT distribution follows a Landau distribution.

Cluster size distribution

The cluster size distribution is one of the important analysis for silicon detectors, in particular for high η measurements and the measurements under external magnetic field.

In general, the size of a cluster should be calculated for the X and Y directions separately, but since the angles used in this thesis are small the total number of pixels in the cluster will be presented below.

Efficiency of the central region of the sensor

Hit reconstruction efficiency is a fundamental feature of a pixel detector. It is defined as the probability of finding a hit close to the track. As it was mentioned earlier, the covering area of the telescope plane is less than the covering area of the DUT ($10.6 \times 21.2mm^2$ versus $16.8 \times 20.4mm^2$) and since the tracks are reconstructed using the hits from the telescope planes only part of the DUT can be evaluated. Note that as mentioned before, the clusters close to dead or noisy pixels are not considered in the analysis.

For a given device the tracking efficiency is calculated as a ratio of the Number of Matched Tracks and the Total Number of Tracks:

$$Efficiency = \frac{NumberofMatchedTracks}{TotalNumberofTracks} \quad (6.1)$$

where

- **“Number of Matched Tracks”** corresponds to the fraction of the total number of tracks that are matched to a hit on the evaluated device. Another important characteristic of the device is the efficiency pixel map which details the efficiency within a single pixel.
- **“Total Number of Tracks”** is the number of reconstructed tracks that have matching hit on at least one other DUT (not the one being evaluated) and that extrapolate to the sensitive area of the DUT being evaluated.

Position resolution

The position resolution for the devices under test is estimated separately for X and Y directions and is based on the evaluation of the residuals:

$$Residual_{X,Y} = TrackPosition_{X,Y} - ClusterCenterPosition_{X,Y} \quad (6.2)$$

There exist several algorithms to define the cluster center:

- **MaxToT:** the center of the cluster is selected at the center of the pixel with highest ToT value.
- **η - correction** - it shows cumulative distribution of some parameter mapped over the pixel area. It is helpful when exploring the behavior of the given parameter in the space between neighboring pixels.
- **Analog:** the center of the cluster is a mean position of the pixels in the cluster, without using the ToT information.
- **Digital:** the cluster center is the ToT weighted center of the cluster.

If a cluster consists of one pixel only, all these algorithms give equal results, and such clusters are of little interest.

Chapter 7

Analysis of test beam's data

In this chapter the data analysis results from March IBL testbeam at DESY of PPS and 3D (FBK) pixel devices are presented.

Efficiency

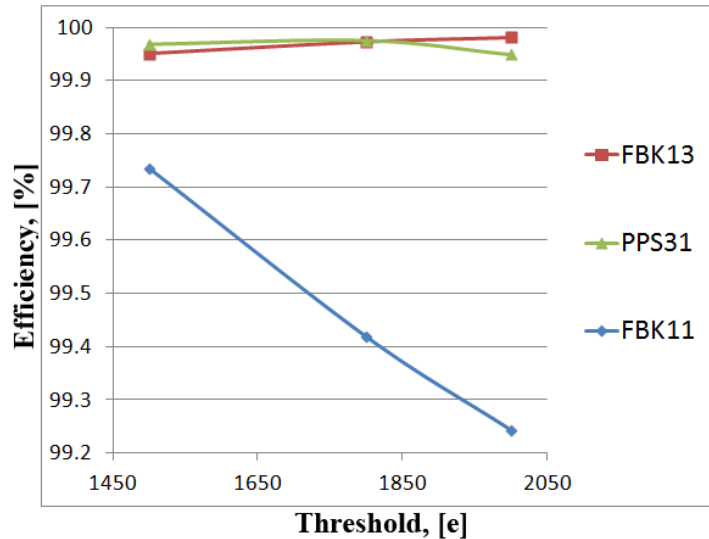


Figure 7.1: Efficiency with constant Bias Voltage depending on Threshold
FBK13: Bias Voltage = 15V, un-irradiated
PPS31: Bias Voltage = 100V, un-irradiated
FBK11: Bias Voltage = 140V, p-irradiated: $6.8 \times 10^{15} n_{eq}/cm^2$

On Figure 7.1 can see good performance of un-irradiated samples FBK13 and PPS31 (>99.9%). For p-irradiated one FBK11 can see, that performance are decreased with increasing of Threshold form $1500e^-$ to $2000e^-$.

It was expected for irradiated devices. It is related with high value of threshold. But even with threshold equals $2000e^-$, performance is still very good (99.2437%).

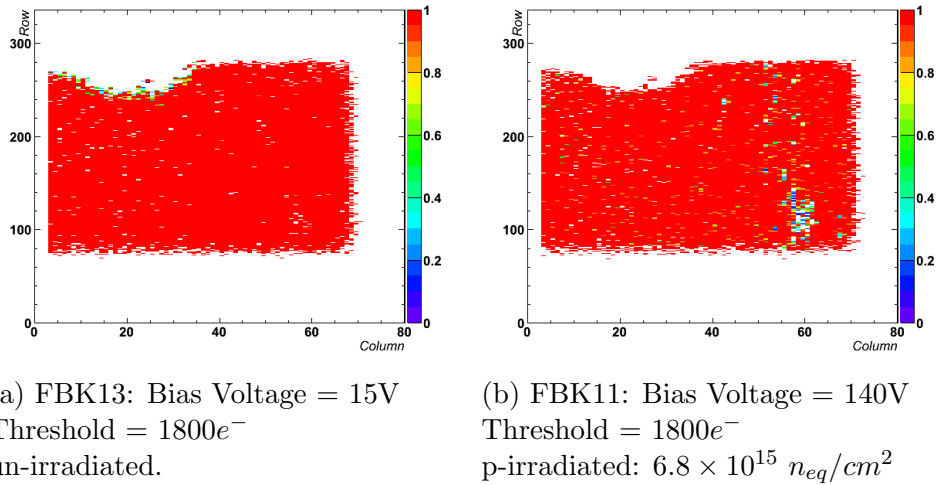


Figure 7.2: Efficiency Sensor Maps

If look on Efficiency Sensor Map of FBK13 sensor (see Fig.7.2, (a)), can see some defect in top left region, it is related with bump bonding problems. FBK11 and FBK13 were in one batch on test beam in DESY (were standing one by one; each time were only two devices on the test beam), that is why, due to the reconstruction process, can see the same defect on Efficiency Sensor Map of FBK11 sensor (see Fig.7.2, (b)).

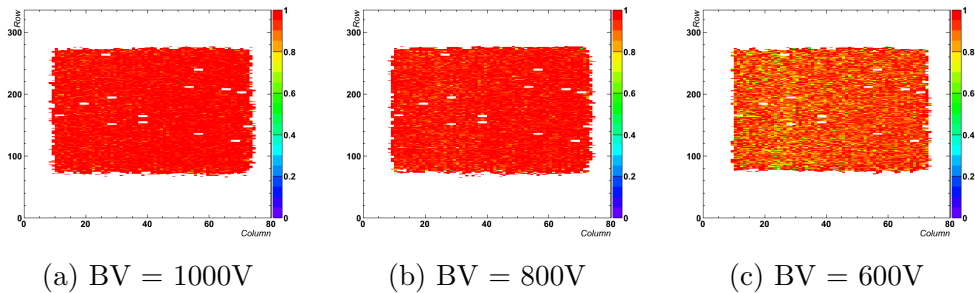


Figure 7.3: Efficiency Sensor Maps for PPS75 depending on BV (Bias Voltage). Threshold = $1500e^-$; p-irradiated: $6.8 \times 10^{15} n_{eq}/cm^2$

On Fig.7.3 can see that efficiency is decreasing with decreasing of bias voltage. It's related with fact, that with increasing of bias voltage depletion

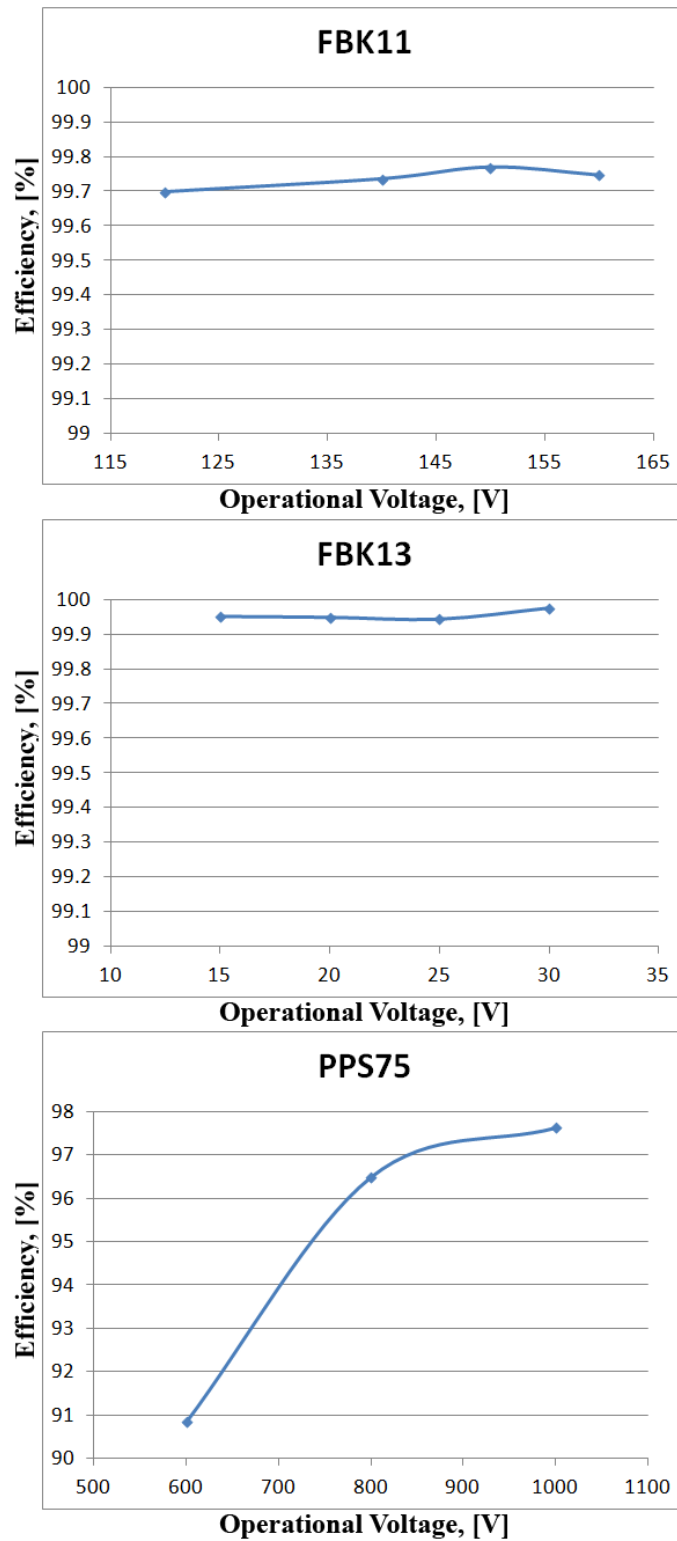


Figure 7.4: Efficiency depends on Bias Voltage, Threshold = $1500e^-$

zone of semiconductor detectors are increasing, and as a result efficiency of detecting is increasing.

LVL1 trigger distribution

In Figure 7.5 the LVL1 trigger distribution plots are presented for the un-irradiated PPS31 and FBK13 and the p-irradiated PPS75 and FBK11. There is no plateau contribution on the plot, which indicates good system synchronization (little noise).

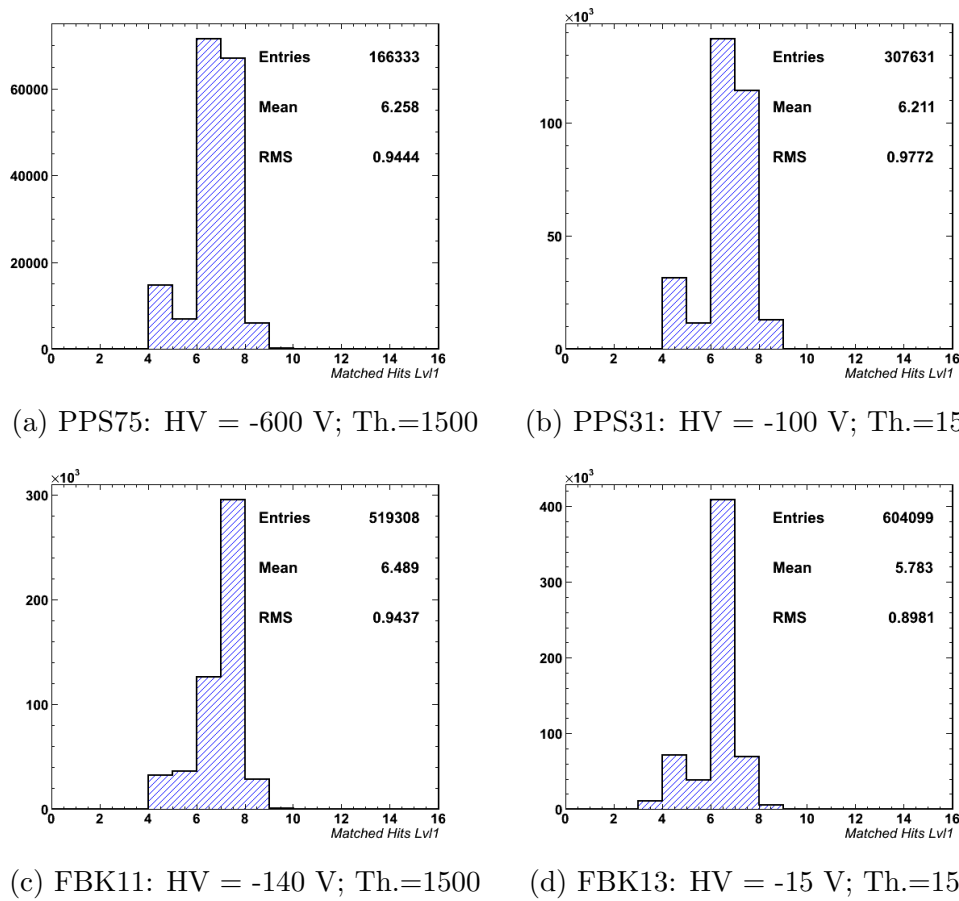
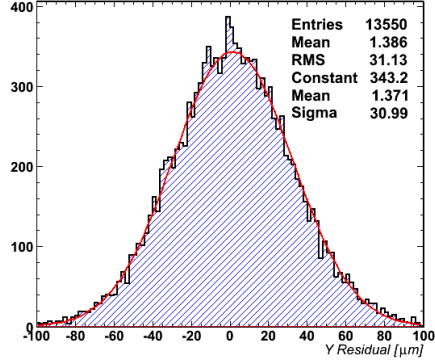


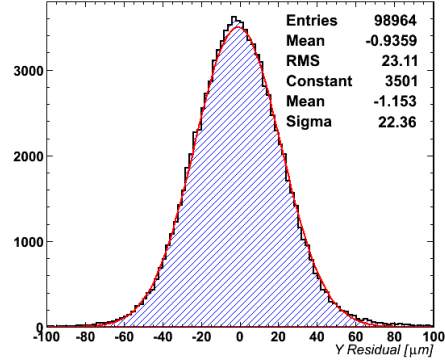
Figure 7.5: LVL1 trigger distribution

Residuals of cluster size 2 in the short(Y) direction

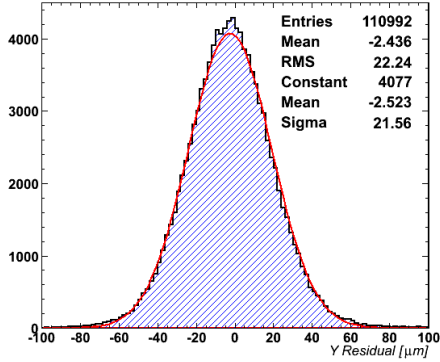
The residuals for cluster size equal to two pixels in the short (Y) direction using the analog cluster center are presented in the Figure 7.6.



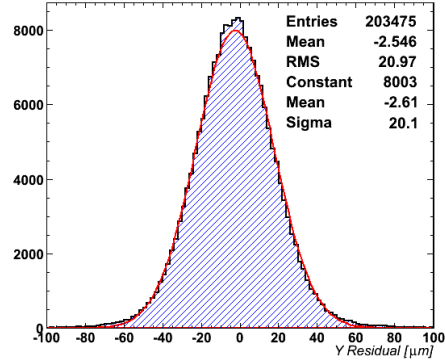
(a) PPS75: HV = -600 V; Th.=1500



(b) PPS31: HV = -100 V; Th.=1500



(c) FBK11: HV = -140 V; Th.=1500



(d) FBK13: HV = -15 V; Th.=1500

Figure 7.6: Residuals for cluster size equal to 2 in short Y direction using analog clustering.

Taking into account that the telescope's contribution to the error is of about $3 \mu m$, one can obtain the approximate resolution for the sensors using equation:

$$\sigma_{DUT} = \sqrt{\sigma^2 - \sigma_{TEL}^2} \quad (7.1)$$

$$\sigma_{DUT(PPS75)} \approx 30.84 \mu m$$

$$\sigma_{DUT(PPS31)} \approx 22.16 \mu m$$

$$\sigma_{DUT(FBK11)} \approx 21.35 \mu m$$

$$\sigma_{DUT(FBK13)} \approx 19.88 \mu m$$

Chapter 8

Conclusions

The ATLAS Collaboration will install a fourth pixel layer in 2013-2014. The IBL will be mounted directly on a new beam pipe at an average radius of 3.3 cm. Two pixel technologies are being evaluated for the IBL, planar and 3D sensors. A possible layout that combines both technologies is under consideration. PPS and 3D-pixel sensor pre-productions have been completed and the devices have been characterized and investigated with beam tests.

The testbeam results indicate that the PPS and 3D devices meet the IBL requirements in terms of hit reconstruction efficiency ($>97\%$) and position resolution after irradiation to a fluency of $5 \times 10^{15} n_{eq}/cm^2$. The optimal parameters for the operation of samples were determined. A threshold of $1500e^-$ and an operational voltage of 150V for FBK11 and 1000V for PPS75 ensure a good performance of the devices.

The results presented in this thesis are important to determine the IBL sensor technology. The good performance of the 3D-pixel and PPS devices has been demonstrated.

Bibliography

- [1] The ATLAS Collaboration, The ATLAS Experiment at the CERN Large Hadron Collider, JINST 3 S08003 (2008).
- [2] ATLAS Collaboration, The ATLAS Inner Detector commissioning and calibration, EPJC 70 (2010) 787.
- [3] ATLAS Insertable B-Layer Technical Design Report, CERN-LHCC-2010-013 ; ATLAS-TDR-019.
- [4] ATLAS Insertable B-Layer Technical Design Report, CERN-LHCC-2010-013 ; ATLAS-TDR-019.
- [5] M.S. Alam, et al., Nucl. Instrum. Methods Phys. Res. A 456, 217 (2001).
- [6] C. Kenney et al., Comparison of 3-D and planar silicon detectors, in Proc. 9th Meeting Division Particles Fields of the American Physical Society, Minneapolis (MN), USA, Aug. 11-15, 1996, pp. 1342-1345.
- [7] D. Haas, Proc. of the LCWS2007, (2007),<http://www.eudet.org>.
- [8] M. Backhaus et al., Development of a versatile and modular test system for ATLAS hybrid pixel detectors, Nucl. Instrum. Meth. A650 (2011) 57 ;37-40. International Workshop on Semiconductor Pixel Detectors for Particles and Imaging 2010.
- [9] <http://root.cern.ch/drupal/>
- [10] I.Rubinskiy. EUDET-Memo-2012-02. EU Telescope. Offline track reconstruction and DUT analysis software, 2012.
- [11] Kyrre Ness Sjobak, Full simulation of a testbeam experiment including modeling of the Bonn Atlas Telescope and Atlas 3D pixel silicon sensors, University of Oslo 2010.
- [12] Jorn Grosse-Knetter, Vertex Measurement at a Hadron Collider - The ATLAS Pixel Detector, BONN-IR-2008-04

- [13] IBL Testbeam March at DESY official web page
<https://twiki.cern.ch/twiki/bin/viewauth/Atlas/IBLTBMarch2012>
- [14] The ATLAS IBL Collaboration, "ATLAS Insertable B-Layer Technical Design Report", CERN-LHCC-2010-013, 2010.
- [15] Rivero Fabio, Characterization of FBK-irst 3D Double Side Double Type Column Silicon Sensors, 2008-2009
- [16] Igor Rubinskiy, An EUDET/AIDA pixel beam telescope for detector development, CERN, 15 February 2012
- [17] S. Grinstein, on behalf of the ATLAS Collaboration, Overview of Silicon Pixel Sensor Development for the ATLAS Insertable B-Layer (IBL), Universitat Autònoma de Barcelona (UAB), E-08193 Bellaterra (Barcelona), Spain, 2011.
- [18] G. Pellegrini, et al., Nucl. Instrum. Methods Phys. Res. A 592, 38 (2008).